

Investigation on Pulse Radiation Characteristics of Discretized Apertures in Time-domain

Binwen Wang, Hui Ning, Chengyun Cao, Qilong Liu, and Kaiyue Zhang

Northwest Institute of Nuclear Technology
Xi'an 710024, China

srhx.bingwen@aliyun.com, ninghuisun@aliyun.com, caochengyun12@163.com,
820091469@qq.com, kaiyo@163.com

Abstract – In view of the challenges and difficulties encountered in the analysis and application of time-driven ultra-wideband array antennas (TD-UWB arrays), this study investigates the pulse radiation characteristics of discretized apertures based on aperture radiation theory and space superposition principle. The impact of discretized aperture linear arrays and planar arrays to restore the radiation of original aperture is examined, along with an analysis of how discretization methods influence the radiated pulse waveforms. The potential application of discretized aperture radiation in research of TD-UWB array antennas is studied, and a method is proposed for predicting time-domain radiation characteristics of TD-UWB arrays. Numerical results demonstrate that the proposed method derived from the discretized aperture radiation can effectively predict the temporal pattern and radiation waveforms of TD-UWB arrays. The research expands and advances the practical applications of aperture radiation, thereby offering a novel perspective for analyzing the radiation characteristics of TD-UWB arrays.

Index Terms – discretized aperture, pulse radiation characteristics, tangential electric field, TD-UWB arrays, time-domain pattern.

I. INTRODUCTION

With the rich frequency components and short-pulse characteristics in time-domain [1], ultra-wideband pulses have demonstrated significant advantages and extensive potential applications in ground penetrating radar [2, 3], high-precision positioning [4, 5], biomedicine [6, 7], wireless communications [8, 9], nondestructive testing [10] and electromagnetic compatibility [11–14] as well as other domains. Sequentially, the ultra-wideband antenna has been a research focus within the field of antenna technology [15–17]. Time-driven ultra-wideband array antenna (TD-UWB array) enhances the radiation gain by increasing the aperture area, while also expanding the capabilities of the radiation sys-

tem through the introduction of multiple spatial degrees of freedom such as beam customization and waveform reconstruction [18]. This approach has emerged as a prominent method for generating and applying ultra-wideband time-domain pulses [19–23]. The radiation of ultra-wideband pulse falls within the realm of transient electromagnetics, which indicates that the study of ultra-wideband array antenna significantly deviates from conventional time-harmonic antennas. The introduction of time variable results in the radiation characteristics of UWB array antennas having dual dependencies on both time and space. In addition, the radiation performances are not only related to the element antenna structure and array scale but also depend on excitation pulse waveforms and delay constraint conditions [21]. Because of the influences of multiple factors, there is a dearth of robust research methodologies for the analysis of ultra-wideband array antennas. Specifically, array pattern synthesis and beamforming pose significant challenges due to the absence of universally applicable field distribution functions.

Analysis of array antennas is closely tied to the array factor, which serves as a concrete representation of the spatial arrangement of the array elements. Foo proposed the temporal array factor to describe the pattern characteristics of UWB array antenna in time-domain [22]. Yan et al. introduced the temporal array factor of planar array with the basis of the three-dimensional impulse point source response, and further proposed the theory of time-domain pattern convolution employing the temporal array factor of isotropic planar array and time-domain pattern of array element [23]. However, the measurements of time-domain pattern and radiation pulses is indispensable in practical applications. The extraction of array factors can solely investigate the impact of array layout and scale on the time-domain pattern. Nevertheless, a complete depiction of time-domain radiation characteristics necessitates integrating the array factors with the radiation characteristics of array elements. Fortunately, aperture radiation encompasses both aspects and

provides a direct assessment of the combined effect. That is the aperture radiation characteristics already demonstrate the influence of both tangential electric field and aperture dimensions, without requiring additional extraction of the array factor. Aperture radiation theory derived from the equivalent source theorem of electromagnetics is an effective means for analyzing the radiation characteristics of aperture antennas [24–26]. Nevertheless, the application of aperture radiation theory on the analysis and prediction of radiation characteristics for TD-UWB arrays remains a technical challenge.

To break the current dilemma and satisfy practical requirements, an investigation is conducted into discretized aperture radiation characteristics. Then the realistic applications of discretized aperture radiation are discussed. Subsequently, a method for rapidly predicting the pulse radiation characteristics of TD-UWB array antennas is proposed, thereby offering a novel approach to analyze TD-UWB arrays. This paper is organized as follows. The first section is the introduction of the research background. The second section reviews the derivation of aperture radiation theory and the solution method in time-domain and presents two discretization approaches for radiation apertures. The third section analyzes the radiation characteristics of the discretized aperture planar arrays. In the penultimate section, the potential applications of discretized aperture radiation are explored and a verified prediction method for pulse radiation characteristics of TD-UWB arrays is proposed. The final section is the conclusion of this paper.

II. APERTURE RADIATION THEORY

A. Derivation of aperture radiation in time-domain

A rectangular aperture is taken as an example to review and derive the aperture radiation field in time-domain. Figure 1 illustrates the radiation diagram of a rectangular aperture, which is positioned in the x - y plane with side lengths a and b . The tangential electric field on the aperture is uniformly distributed in the y direction. Point P represents the external field point of the radiation aperture. To differentiate the source point and field point, the coordinates of source points are denoted by a superscript.

Based on the surface equivalent source theorem, an ideal conductor is chosen as the medium within the aperture, allowing only for consideration of the equivalent magnetic current contribution on the aperture surface [27]. The equivalent magnetic current on the aperture surface can be obtained from the tangential electric field:

$$\vec{J}_m = -\vec{n} \times \vec{E}_t, \quad (1)$$

where \vec{n} is the unit vector in the normal direction of the aperture and \vec{E}_t refers to the tangential electric field.

Ignoring the edge effect of radiation aperture, the electric field at external field point can be obtained by

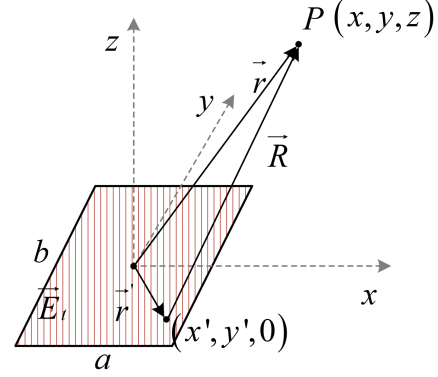


Fig. 1. Radiation diagram of the rectangular aperture.

Maxwell's equations with magnetic current source:

$$\vec{E}(\vec{r}, t) = \frac{1}{4\pi} \int_S \nabla \times \left(\vec{n} \times \frac{\vec{E}_t(\vec{r}', t - R/c)}{R} \right) ds', \quad (2)$$

where R refers to the distance between field point and source point.

Employing a series of vector analysis to simplify the integral term in equation (2), the electric field radiated from the equivalent magnetic source is derived as follows:

$$\vec{E}(\vec{r}, t) = \frac{1}{4\pi} \int_S \left\{ \begin{array}{l} -\vec{n} \cdot \left[\frac{\vec{R}}{cR^2} \frac{\partial \vec{E}_t(\vec{r}', t - \frac{R}{c})}{\partial t} + \frac{\vec{E}_t(\vec{r}', t - \frac{R}{c}) \cdot \vec{R}}{R^3} \right] + \\ \vec{n} \cdot \left[\frac{\vec{R} \vec{E}_t(\vec{r}', t - \frac{R}{c})}{R^3} + \frac{\vec{R}}{cR^2} \frac{\partial \vec{E}_t(\vec{r}', t - \frac{R}{c})}{\partial t} \right] \end{array} \right\} ds'. \quad (3)$$

It is assumed that the tangential electric field on the aperture is denoted as:

$$E_t(\vec{r}', t - \frac{R}{c}) = f\left(\vec{r}', t - \frac{R}{c}\right). \quad (4)$$

Then, the radiated electric field expressions in difference polarizations at external field point are presented:

$$E(\vec{r}, t) \vec{e}_y = \frac{-1}{4\pi c} \int_S \left[\frac{(z-z')}{R^2} \cdot \frac{\partial f(\vec{r}', t - \frac{R}{c})}{\partial t} + \frac{c(z-z')}{R^3} f\left(\vec{r}', t - \frac{R}{c}\right) \right] ds', \quad (5)$$

$$E(\vec{r}, t) \vec{e}_z = \frac{1}{4\pi c} \int_S \left[\frac{(y-y')}{R^2} \cdot \frac{\partial f(\vec{r}', t - \frac{R}{c})}{\partial t} + \frac{c(y-y')}{R^3} f\left(\vec{r}', t - \frac{R}{c}\right) \right] ds'. \quad (6)$$

The results illustrate that the tangential electric field in y direction generates two kinds of electric field components in orthogonal polarization directions. The electric field in y direction is the principal polarization component, which is the focus to be investigated. Additionally, it can be clearly observed from the electric field expressions that the distribution of the tangential electric field and the aperture dimensions are key points to determine the radiated pulse waveforms and amplitude. Specifically, there are many variations of the tangential electric fields, which is exactly the emphasis and significance to utilize the aperture radiation theory to conduct realistic problems.

The integration is transformed into summation through discretization approach to calculate the principal polarized electric field [28]. Firstly, the time variable is represented as follows:

$$t = n\Delta t + \frac{R}{c}. \quad (7)$$

Then, the discretization forms of equation (5) are conducted as:

$$E\left(\vec{r}, n\Delta t + \frac{R}{c}\right) \vec{e}_y = \sum_{i,j} \begin{bmatrix} A_{i,j} f((n+1)) \\ + B_{i,j} f(n) \\ + C_{i,j} f((n-1)) \end{bmatrix} \Delta x \Delta y, \quad (8)$$

where Δt refers to the time step, $\Delta x \Delta y$ is the cell area in summation, and other coefficients are defined as follows:

$$\begin{cases} A_{i,j} = \frac{1}{4\pi c} \frac{(z-z'_i)}{2\Delta t R^2}, B_{i,j} = \frac{1}{4\pi c} \frac{c(z-z'_i)}{R^3} \\ C_{i,j} = -\frac{1}{4\pi c} \frac{(z-z'_i)}{2\Delta t R^2} \end{cases}. \quad (9)$$

Furthermore, rounding operation is conducted on equation (8), and a new coefficient α is introduced:

$$\alpha = n + \frac{R}{c\Delta t} - n^* \Big|_{n^* = \text{round}(n + \frac{R}{c\Delta t})}. \quad (10)$$

The new coefficient describes the relationship between radiated electric field in different moments, which is the propagation characteristics of transient electromagnetic waves:

$$\begin{cases} E(\vec{r}, n^*) = (1 - \alpha) E(\vec{r}, n + \frac{R}{c\Delta t}) \\ E(\vec{r}, n^* + 1) = \alpha E(\vec{r}, n + \frac{R}{c\Delta t}) \end{cases}. \quad (11)$$

Finally, the discretized calculation expressions for principal polarized electric field are derived as:

$$\begin{cases} E(\vec{r}, n^* - 1) = \sum_{i,j} [(1 - \alpha) A_{i,j} f_2(n)] \Delta x \Delta y \\ E(\vec{r}, n^*) = \sum_{i,j} \begin{bmatrix} (1 - \alpha) B_{i,j} f_2(n) \\ + \alpha A_{i,j} f_2(n) \end{bmatrix} \Delta x \Delta y \\ E(\vec{r}, n^* + 1) = \sum_{i,j} \begin{bmatrix} (1 - \alpha) C_{i,j} f_2(n) \\ + \alpha B_{i,j} f_2(n) \end{bmatrix} \Delta x \Delta y \\ E(\vec{r}, n^* + 2) = \sum_{i,j} [\alpha C_{i,j} f_2(n)] \Delta x \Delta y \end{cases}. \quad (12)$$

It is worth mentioning that the time step in the above calculations must be much less than the rise time or fall time of the excitation pulse. The derived expressions are the specific calculation process of the electric field, not

the aperture discretization involved in this paper. In the next section, the aperture discretization methods will be discussed in detail.

B. Aperture discretization approach

The aperture radiation process and expressions of its radiated electric field show that there are two kinds of discretization approaches for radiation aperture.

The first approach is focused on the discretization to the tangential electric field distribution function. That means, the tangential electric field with different amplitudes and time sequences on different aperture positions are expressed by special functions. With the basis of above analysis, the tangential electric field in equation (4) can be represented as follows:

$$f\left(\vec{r}, t\right) = f_1\left(\vec{r}\right) f_2\left(t - t_d\left(\vec{r}\right)\right), \quad (13)$$

where f_1 refers to the amplitude function of the tangential electric field varying with positions, and t_d describes the time delay between different source points.

Let us take a simple example to demonstrate the calculation of radiated electric field. It is assumed that the amplitudes of the tangential electric field on the aperture vary along the x direction, and the time delay for each source point is the ratio between source point coordinate x' and light velocity. Then, equation (5) can be further crystallized:

$$E(\vec{r}, t) \quad (14)$$

$$= \frac{-1}{4\pi c} \int_s \left[\frac{(z-z')}{R^2} \cdot \frac{f_1(\vec{r}) \partial f(t - \frac{x'}{c} - \frac{R}{c})}{\partial t} + \frac{c(z-z')}{R^3} f_1(\vec{r}) f\left(t - \frac{x'}{c} - \frac{R}{c}\right) \right] ds'.$$

To simplify the practical calculation, the time delay term can be denoted as:

$$x'_i = m_i c \Delta t. \quad (15)$$

Next, the radiated electric field of the aperture excited by discretized tangential electric field can be calculated as:

$$\begin{cases} E(\vec{r}, n^* - 1) = \sum_{i,j} [(1 - \alpha) A_{i,j} f_1(i, j) f_2(n - m_i)] \Delta x \Delta y \\ E(\vec{r}, n^*) = \sum_{i,j} \begin{bmatrix} \alpha A_{i,j} f_1(i, j) f_2(n - m_i) + \\ (1 - \alpha) B_{i,j} f_1(i, j) f_2(n - m_i) \end{bmatrix} \Delta x \Delta y \\ E(\vec{r}, n^* + 1) = \sum_{i,j} \begin{bmatrix} \alpha B_{i,j} f_1(i, j) f_2(n - m_i) + \\ (1 - \alpha) C_{i,j} f_1(i, j) f_2(n - m_i) \end{bmatrix} \Delta x \Delta y \\ E(\vec{r}, n^* + 2) = \sum_{i,j} [\alpha C_{i,j} f_1(i, j) f_2(n - m_i)] \Delta x \Delta y \end{cases}. \quad (16)$$

Equation (16) shows that, when taking the first approach to solve the discretized aperture radiation characteristics, the amplitude matrix of the tangential electric field should be given in advance. Time delay should be transformed into m_i . If the time delay varies along both x and y directions, the matrix of time delay is necessary written as m_{ij} . These operations ahead of radiation calculation brings additional complexities, resulting in obvious inconveniences.

The second discretization approach can be derived from TD-UWB array antennas. The key point is dividing the original aperture into several small apertures with the same area. Employing the calculation method in section II.A, the radiated electric field of arbitrary small aperture with uniform tangential electric field can be calculated easily. Then, simple translations are conducted to obtain the electric field waveforms radiated by small apertures at the external field point. The translations are determined by distances between field point and the centers of these small apertures. It should be noted that, the amplitudes and time delays of the tangential electric fields for each small aperture can also be considered in the translation operations. The final step is space superposition, and the radiated electric field is calculated as follows:

$$\vec{E}(\vec{r}, t) \vec{e}_y = \sum_i^N f_i \vec{E}_i(\vec{r}_i, t - t_{di}) \vec{e}_y, \quad (17)$$

where f_i refers to the tangential electric field amplitude of the i_{th} small aperture, \vec{E}_i refers to the radiated electric field at the external field point of the i_{th} small aperture, and t_{di} is the time delay of the corresponding small aperture.

Compared with the first discretization approach, the second approach obviously simplifies the calculations by putting the operations to amplitude and time delay of small aperture in the middle step, and the physical meaning of the time delay distribution is clearer.

III. DISCRETIZED APERTURE RADIATION CHARACTERISTICS

The calculation expressions of radiated electric field and the physical process of aperture radiation illustrate that the number of integral cells decreases after discretization operations, leading to an increase of the calculation efficiency. However, how to discretize the aperture reasonably and the corresponding discretized aperture radiation performances are significant problems to investigate. Therefore, an example is employed to further verify and illustrate the radiation characteristics of the discretized aperture array.

It is assumed that there is a rectangular aperture as shown in Fig. 1 with side lengths of 1.2 m and 0.6 m. The second discretization approach is operated on this aperture to obtain two discretized aperture linear arrays and three discretized aperture planar arrays. Typical discretized arrays are drawn in Fig. 2. Other discretized array parameters are listed in Table 1.

Two Gaussian pulses with pulse widths of 0.6 ns and 1 ns are employed as the tangential electric field as shown in Fig. 3. All tangential electrical fields are uniformly distributed in each discretized aperture, so as to study the differences and connections between the radiation characteristics of the single and these discretized aperture arrays.

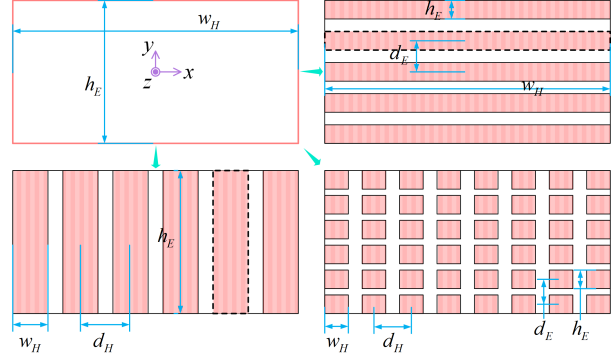


Fig. 2. Typical discretization of the rectangular aperture.

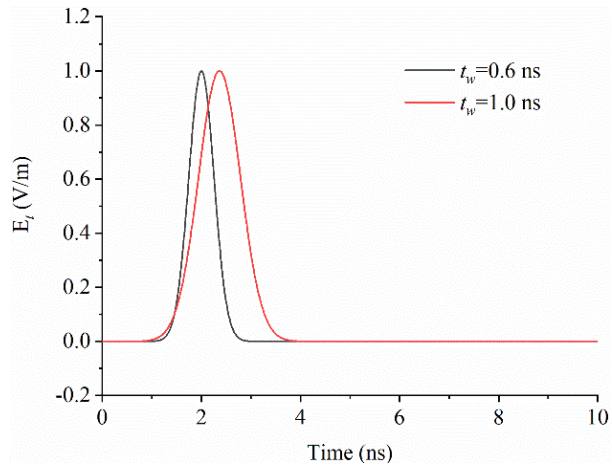


Fig. 3. Two Gaussian pulses with different pulse widths.

Table 1: Array parameters of discretized aperture arrays

No.	1	2	3	4	5	6
Type	Single	Linear		Planar		
Row	1	5	1	3	6	12
Column	1	1	6	4	8	12
h_E/m	0.60	0.08	0.60	0.18	0.075	0.028
w_H/m	1.20	1.20	0.15	0.27	0.115	0.056
d_E/m	—	0.13	—	0.21	0.105	0.052
d_H/m	—	—	0.21	0.31	0.155	0.104

According to the calculation method outlined in section II, the radiation field waveforms of each aperture excited by different tangential electric field pulses are obtained and compared. Specifically, Figs. 4 and 5 illustrate a comparison of radiation field waveforms at three field points radiated by apertures 1 and 4 under different excitation pulses. The coordinates of these three field points are (0,0,10), (8,0,10), and (8,8,10), respectively.

Figures 4 and 5 demonstrate intuitively that the field waveform characteristics of discretized aperture planar

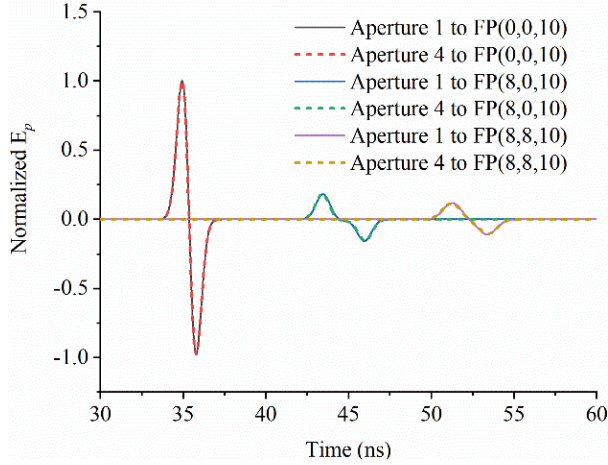


Fig. 4. Electric field waveforms of aperture 1 and 4 excited by Gaussian pulse with pulse width of 1 ns.

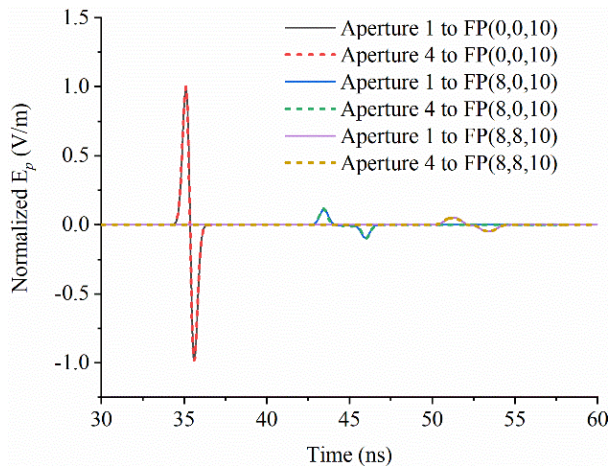


Fig. 5. Electric field waveforms of aperture 1 and 4 excited by Gaussian pulse with pulse width of 0.6 ns.

array 4 at three field points are essentially consistent with those of aperture 1 when excited by the same tangential electric field distributions.

To provide a more general comparison, the radiation field waveforms of aperture 1 are taken as references at each field point, and the pulse mean square error (pulse RMS) is utilized to quantify the impact of aperture discretization on the radiation field waveform. The calculation for pulse RMS is as follows [29]:

$$\sigma = \sqrt{\frac{\int_T \left[\frac{E_i(t)}{|E_i(t)|_{\max}} - \frac{E_0(t)}{|E_0(t)|_{\max}} \right]^2 dt}{\int_T \left(E_0(t) / |E_0(t)|_{\max} \right)^2 dt}}, \quad (18)$$

where E_i and E_0 refer to the electric field waveforms of the i_{th} aperture and the aperture 1, E_{imax} and E_{0max} are the corresponding electric field amplitudes, and T represents the duration time. According to equation (18), the pulse

RMS of the radiation field waveforms for each aperture relative to aperture 1 can be computed under varying tangential electric fields, as illustrated in Fig. 6.

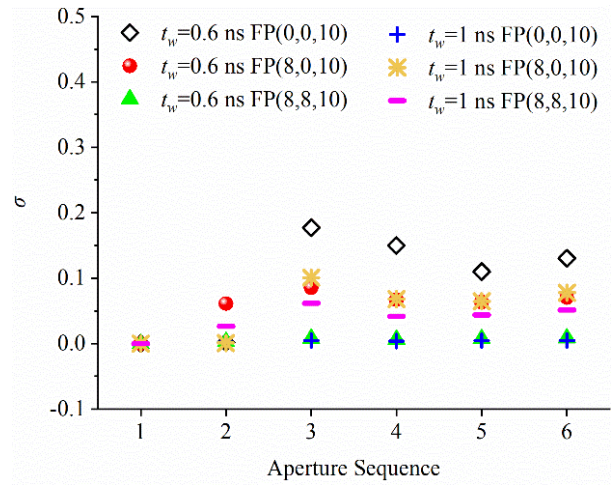


Fig. 6. The pulse RMS of the electric field waveforms for each aperture excited by Gaussian pulses.

As observed from Fig. 6, the discretization to the rectangular aperture introduces a slight distortion to the waveforms of the radiation field. The extent of this distortion is dependent on both the tangential electric field and the chosen approach of discretization. This phenomenon can be analyzed by the principles and processes involved in aperture radiation. Specifically, when an aperture is decomposed into a discretized aperture array, empty gaps devoid of tangential electric field distribution emerge between individual element apertures. These gaps, illustrated in Fig. 2, do not contribute to the overall radiation field and consequently result in discontinuities during superposition with adjacent aperture cells. Consequently, a subtle waveform distortion becomes apparent. Furthermore, this distortion is influenced by both the tangential electric fields and the size of these blank gaps. In other words, for tangential electric fields of different pulse widths, it may be possible to select an appropriate gap size or discretization method that closely approximates the radiation performances of the original aperture.

The above analysis suggests that reasonable selection of discretized aperture can be further investigated by incorporating the following variables:

$$D_c = \frac{\sqrt{d_E^2 + d_H^2}}{\tau c}, \quad (19)$$

where τ is the time constant of the Gaussian pulse and c denotes the speed of light.

Taking aperture 4 and 6 as examples, the variation curves of pulse RMS of radiation field waveform versus

D_c at the field point of (8,8,10) under different tangential electric field pulses are solved and compared in Figs. 7 and 8.

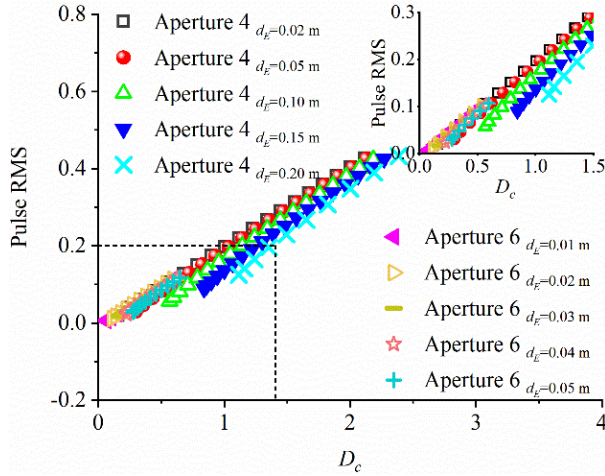


Fig. 7. Radiated pulse RMS at (8,8,10) of aperture 4 and 6 excited by Gaussian pulse with pulse width of 1 ns.

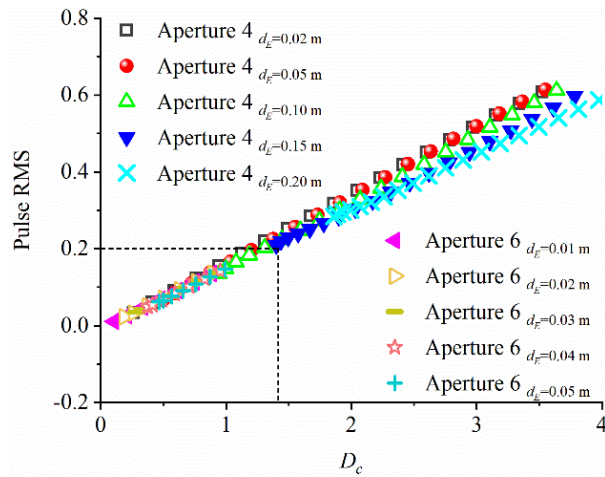


Fig. 8. Radiated pulse RMS at (8,8,10) of aperture 4 and 6 excited by Gaussian pulse with pulse width of 1 ns.

The raising of D_c leads to a linear increase of the pulse RMS as observed from Figs. 7 and 8, which means the distortion is more serious. When D_c is below 1.4, all pulse RMS are less than 0.2. These results demonstrate that when employing a discretized aperture planar array to restore the original aperture for reducing computation consumption, certain conditions must be met to ensure close resemblance to the radiation field waveforms of original aperture.

Despite the calculations and comparisons of radiation field waveforms, an investigation into the temporal pattern of each aperture is also conducted. Figure 9

depicts the E-plane and H-plane time-domain patterns of each aperture excited by the Gaussian pulse with pulse width of 1 ns.

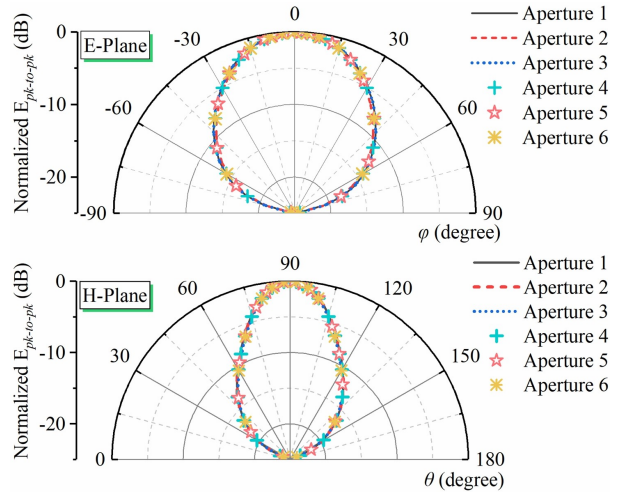


Fig. 9. Time-domain patterns of each aperture excited by the tangential electric field with pulse width of 1 ns.

The time-domain patterns in E-plane and H-plane of each aperture exhibit a relatively consistent behavior when excited by the same tangential electric field waveforms. This indicates that the discretized aperture planar arrays still retain original pattern characteristics, which essentially correspond to the array factor. Discretization accurately restores the array factor of the original aperture. In general, more emphasis is placed on the 3-dB beam width. The differences of each aperture’s 3-dB beam width with respect to aperture 1 are depicted in Fig. 10.

In the case of the planar array, apertures 4, 5, and 6 exhibit distinct differences in time-domain patterns compared to aperture 1, as clearly depicted in Fig. 10. However, for the linear array, both the H-plane pattern of aperture 2 and the E-plane pattern of aperture 3 remain consistent with that of aperture 1. This indicates that the discretizing way of linear array effectively preserves the array factor in respective planes. Consequently, two additional small apertures (aperture 7 and aperture 8) are constructed for further analysis. They are the dashed boxes in Fig. 2. The dimensions of aperture 7 are $w_H=1.2$ m and $h_E=0.1$ m, while those of aperture 8 are $w_H=0.1$ m and $h_E=0.6$ m.

Figure 11 presents the calculated time-domain patterns for these two apertures excited by a tangential electric field with pulse width of 1 ns. The time-domain pattern in H-plane of aperture 7 is observed to be nearly identical to that of aperture 1, while the pattern in E-plane of aperture 8 closely resembles that of aperture 1.

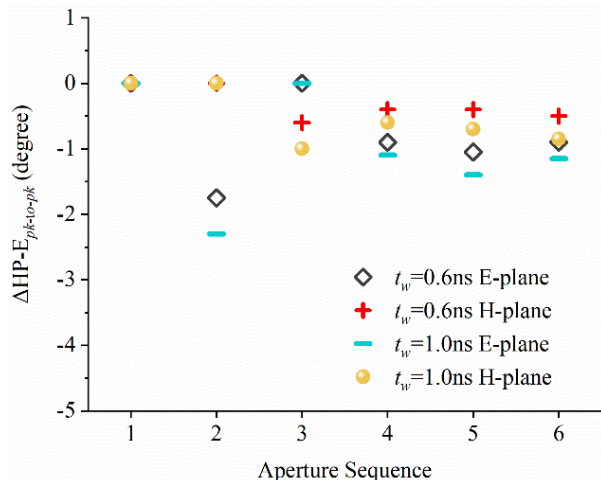


Fig. 10. The differences of the 3-dB beam width with respect to aperture 1.

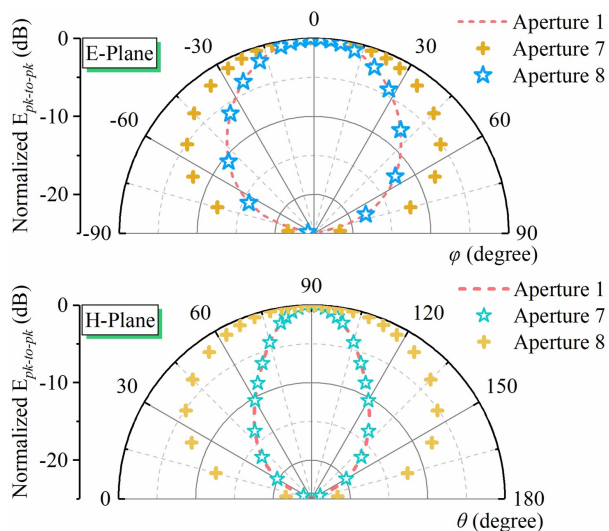


Fig. 11. Time domain patterns of aperture 7 and 8.

This suggests that the time-domain pattern in the corresponding plane can be equivalently calculated using two smaller apertures.

When a Gaussian pulse with pulse width of 1 ns and an amplitude of 1 kV/m is employed as the tangential electric field waveform, the comparisons between the electric field waveforms radiated by these apertures at typical field points are made in Fig. 12. The change in the number of integral aperture elements leads to a modification in the amplitude of the radiation electric field. Therefore, the ratio between the area of new constructed aperture and aperture 1 is employed as an amplitude coefficient, enabling us to obtain the complete waveform of the radiation field.

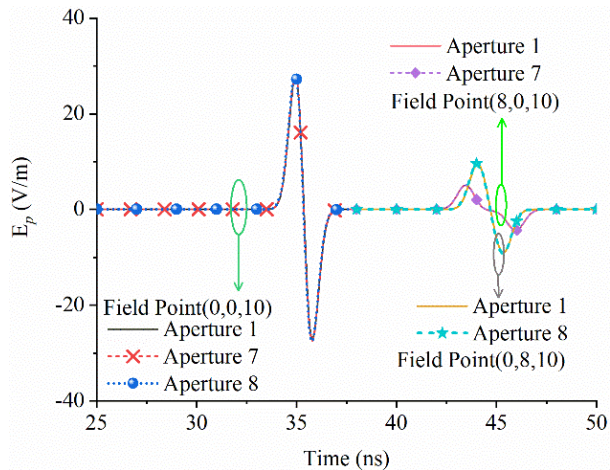


Fig. 12. The radiated electric field waveforms at typical field point.

Figure 12 clearly shows that the accurate calculation of the radiation field waveform at the field points on the E-plane and H-plane can be achieved by utilizing two narrow apertures. This is attributed to the symmetric time delay effect caused by the distance R between the field and source points when solving for the radiation field waveform at either E-plane or H-plane. In other words, the radiation field waveform at a given field point in E-plane or H-plane solely depends on the source point located in that respective plane.

IV. ANALYSIS AND DISCUSSION OF POTENTIAL APPLICATIONS

This section focuses on exploring potential applications of discretized aperture for analyzing TD-UWB array antennas. Figure 13 (a) depicts an antipodal Vivaldi antenna with the dimensions indicated, which is a typical UWB antenna. The dielectric substrate utilized is FR4, with the relative dielectric constant of 4.3 and loss tangent of 0.025. Employing the antipodal antenna as the array element, an 8×8 time-driven array is constructed as illustrated in Fig. 13 (b). The spacing between array elements on the E-plane is $d_E=0.27$ m, while on the H-plane the spacing is $d_H=0.15$ m. The reduced scale of this array antenna aims to alleviate computational burden during numerical simulations.

Based on the aperture radiation theory, there are two crucial factors for predicting the time-domain radiation characteristics of the TD-UWB arrays. The first is the equivalent aperture, while the second is the tangential electric field on the aperture. According to the analysis in section III, two narrow apertures can be employed separately to solve and estimate the time-domain radiation characteristics of this array antenna under synchronous excitation mode. The dimensions of these two narrow

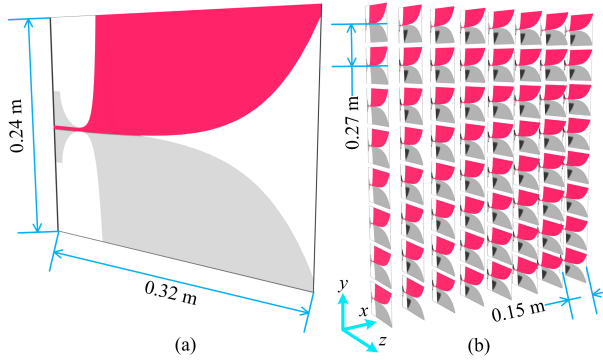


Fig. 13. The antipodal Vivaldi antenna and the 8×8 array antenna.

apertures are 1.2 m × 0.1 m (aperture E) and 0.1 m × 2.16 m (aperture H), respectively.

According to the radiation process of the array antenna, the tangential electric field of its equivalent aperture is an intermediate quantity that relies on both the excitation pulse of the array antenna and element antenna structure. Also, it serves as the source for the aperture radiation field. For simplicity, numerical simulation based on finite integral techniques is employed to obtain the tangential electric field waveform. First, to construct a 5×5 subarray, the layout of which is the same as the 8×8 array antenna in Fig. 13 (b). Then, the electric field in the reactive near-field region of the middle element of the subarray is extracted and serves as the tangential electric field on the aperture surface. This operation has taken the mutual coupling of the array elements into account. It is assumed that the excitation pulse is still the Gaussian pulse with pulse width of 1 ns and amplitude of 7.07 V/m. The extracted tangential electric field waveform by numerical simulation is displayed in Fig. 14.

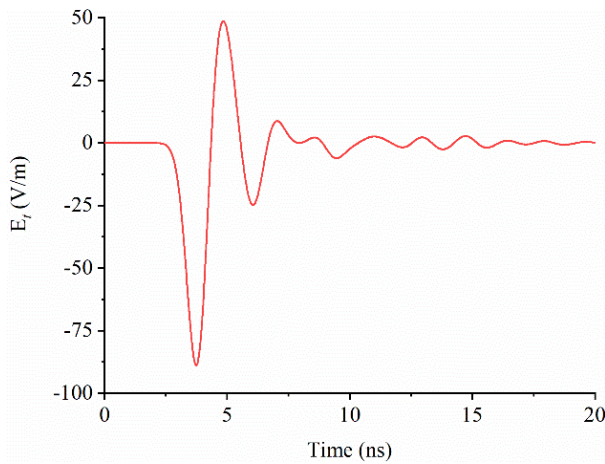


Fig. 14. The extracted tangential electric field waveform.

The distribution of tangential electric field on the radiation aperture surface of the array antenna is non-uniform. This means that there exists a certain amplitude and time delay distribution of tangential electric fields on the equivalent aperture. However, for simplicity purposes, the uniform distribution of tangential electric field on each narrow aperture is assumed as the precondition. Then, the time-domain patterns in E-plane and H-plane of the 8×8 array antenna are predicted, employing aperture E and H, as illustrated in Fig. 15.

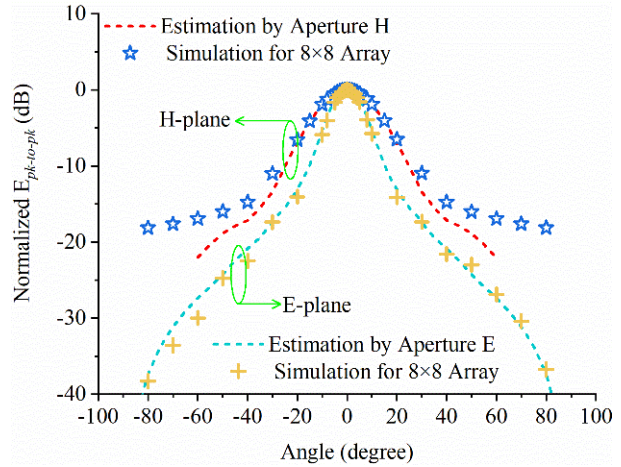


Fig. 15. The predicted time-domain patterns in the H-plane and E-plane of the 8×8 array antenna.

As can be clearly seen from Fig. 15, the time-domain pattern in E-plane predicted by aperture E (2.16 m × 0.1 m) exhibits excellent agreement with the simulated results of the 8×8 array antenna, while for the H-plane pattern, the agreement is only observed within the range of ±30°. However, notable disparities emerge beyond this range due to the fact that the prediction solely considers radiation contributions from the front of the array, whereas there are additional contributions emitted by the side array elements outside ±30° in numerical simulations. Remarkably, considering that the 3-dB beam width in H-plane is merely ±12°, these findings adequately meet estimation requirements.

Additionally, the radiation field waveforms at typical field points can be accurately predicted using the two narrow apertures, as depicted in Figs. 16 and 17. The radiated electric field waveforms predicted by the two narrow apertures exhibit remarkable concordance with the numerical results in terms of both amplitude and waveform characteristics. This further exemplifies the efficacy of utilizing narrow apertures to predict the radiation characteristics of array antenna.

Similar to phased arrays, TD-UWB array antennas are capable of beam scanning. In this case, the narrow aperture can be discretized to predict the time-domain

pattern during beam scanning mode. For instance, when the 8×8 array antenna operates in beam scanning mode in E-plane, the aperture E is discretized into an 8×1 linear array consisting of small apertures measuring $0.24 \text{ m} \times 0.1 \text{ m}$.

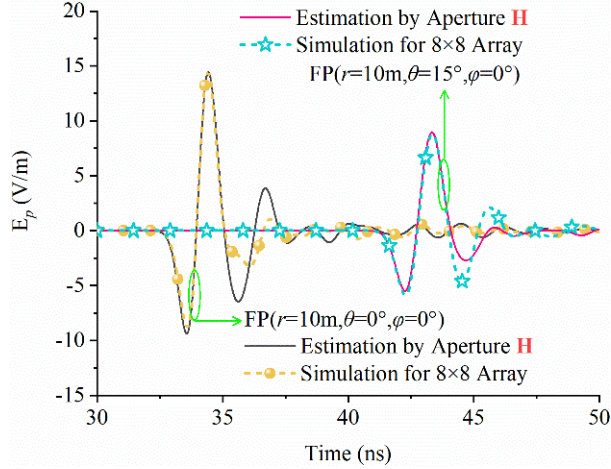


Fig. 16. The electric field waveforms at two field points predicted by aperture H.

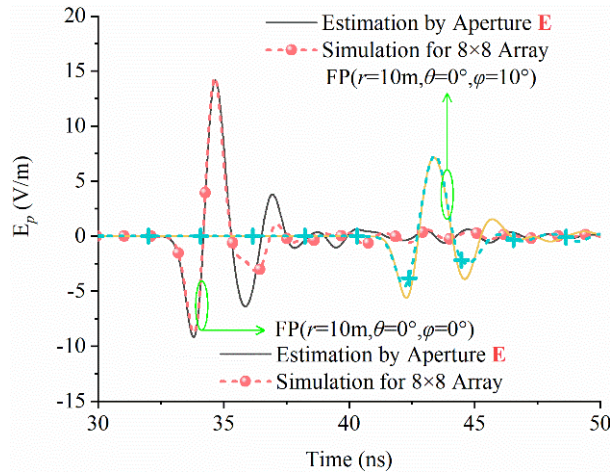


Fig. 17. The electric field waveforms at two field points predicted by aperture E.

The waveform shown in Fig. 14 is still utilized as the excitation tangential electric field, but the excitation time sequence (i.e., t_{di} in equation (17)) is reset according to beam scanning mode [30]. The time-domain patterns operating in E-plane beam scanning mode are predicted and compared with simulated results, as depicted in Fig. 18. Notably, the field strengths working in beam scanning mode are normalized relative to that of principal axis radiation field strength during synchronous excitation.

Figure 18 demonstrates that the time-domain patterns in E-plane with different scanning angles are all in good agreement with the simulated results. Moreover, it is observed that the field strength on the principal axis decreases as the scanning angle increases. The quantitated results for both 3-dB beam widths and scanning angles are presented in Table 2.

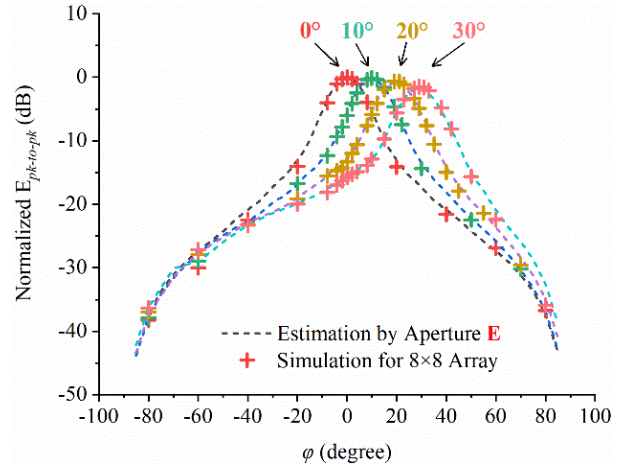


Fig. 18. Comparisons of time-domain patterns in E-plane beam scanning mode.

Table 2: The quantitated results of time-domain pattern in E-plane beam scanning mode

Time delay/ns	0	0.16	0.31	0.45
Desired angle/ $^{\circ}$	0	10.24	20.15	30.00
Simulated angle/ $^{\circ}$	0	10.00	20.00	29.00
Simulated BW/ $^{\circ}$	13.54	13.95	14.69	15.90
Predicted angle/ $^{\circ}$	0	10.00	19.00	28.00
Predicted BW/ $^{\circ}$	14.63	14.86	15.57	16.26

The results presented in Table 2 demonstrate a close agreement between the predicted scanning angles and both the simulated and desired values. Although the predicted 3-dB beam width (BW) slightly exceeds the numerical results, the consistent trend suggests that this method is suitable for analyzing radiation characteristics of TD-UWB arrays operating on beam scanning mode. Additionally, Fig. 19 compares the predicted and simulated radiation field waveforms at two different field points when the beam scanning angle is set to 20° .

Figure 19 demonstrates that the method can also correctly predict the amplitude and oscillating characteristics of electric field waveforms for the TD-UWB array within beam scanning mode.

In this section, the tangential electric field waveform on the equivalent aperture is extracted by numerical simulation to simplify the whole prediction process,

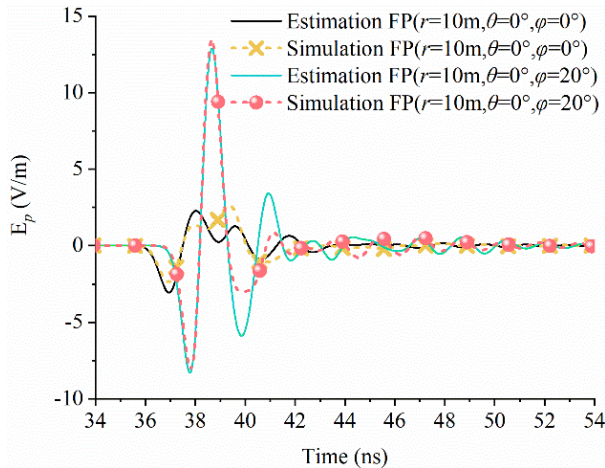


Fig. 19. The predicted radiated electric field waveforms at typical field points (FP) with the E-plane beam scanning angle of 20° .

and aimed to demonstrate the potential applications of discretized aperture radiation. There are various methods to obtain equivalent tangential electric field waveforms, such as using normalized waveforms or combining impulse responses with measured radiation fields for inversion. All of these approaches allow for predicting time-domain patterns and radiated electric fields of TD-UWB array antennas through aperture radiation, enabling further study and design of TD-UWB arrays and facilitating pattern synthesis.

V. CONCLUSION

Aperture radiation theory is derived from the equivalent source theorem of electromagnetics, which provides an effective approach for analyzing the radiation characteristics of array antennas. This paper presents a comprehensive review of the derivation process and solution method for aperture radiation theory. Various discretized aperture planar arrays were constructed to investigate the radiation characteristics, such as waveform analysis, pulse mean square error evaluation, and time-domain pattern examination. The results demonstrate that a reasonable discretization accurately reflects and restores the radiation characteristics of the original aperture while significantly improving computational efficiency through reduced integral surface elements. Moreover, employing narrow apertures with dimensions identical to the original aperture in E-plane or H-plane enables rapid calculation of radiation field waveforms and time-domain patterns within these planes. Building upon the analysis of discretized aperture radiation, the potential applications in TD-UWB array antennas are discussed, and a fast method for predicting the time-domain radiation characteristics of TD-UWB arrays is

proposed and validated through numerical simulation. The findings and research expand upon practical applications of aperture radiation theory while providing novel ideas and methods for analysis and design of TD-UWB arrays. Furthermore, the proposed method can serve as a foundation for array antenna synthesis while offering guidance towards engineering implementation.

REFERENCES

- [1] R. J. Fontana, "Recent system applications of short-pulse ultra-wideband (UWB) technology," *IEEE Trans. Microwave Theory Tech.*, vol. 52, no. 9, pp. 2087-2104, Sep. 2004.
- [2] T. Saeidi, A. R. H. Alhawari, A. H. M. Almwagani, T. Alsuwian, M. A. Lmrnan, and Q. Abbasi, "High gain compact UWB antenna for ground penetrating radar detection and soil inspection," *Sensors*, vol. 22, no. 14, p. 5813, July 2022.
- [3] J. Guo, J. Tong, Q. Zhao, J. Jiao, J. Huo, and C. Ma, "An ultrawide band antipodal Vivaldi antenna for airborne GPR application," *IEEE Geosci. Remote Sens. Lett.*, vol. 16, no. 10, pp. 1560-1564, Oct. 2019.
- [4] M. Elsanhoury, P. Mäkelä, J. Koljonen, P. Välisuo, A. Shamsuzzoha, T. Mantere, M. Elmusrati, and H. Kuusniemi, "Precision positioning for smart logistics using ultra-wideband technology-based indoor navigation: A review," *IEEE Access*, vol. 10, pp. 44413-44445, Apr. 2022.
- [5] W. Wang, D. Marelli, and M. Fu, "Multiple-vehicle localization using maximum likelihood Kalman filtering and ultra-wideband signals," *IEEE Sens. J.*, vol. 21, no. 4, pp. 4949-4956, Oct. 2020.
- [6] I. M. Danjuma, M. O. Akinsolu, C. H. See, R. A. Alhameed, and B. Liu, "Design and optimization of a slotted monopole antenna for ultra-wide band body centric imaging applications," *IEEE J. Electromagn. RF Microwaves Med. Biol.*, vol. 4, no. 2, pp. 140-147, June 2020.
- [7] A. Martínez, C. Blanco, H. García, R. Gutiérrez, G. Torregrosa, E. Ávila, and J. M. Sabater, "UWB-printed rectangular-based monopole antenna for biological tissue analysis," *Electronics*, vol. 10, no. 3, p. 304, Jan. 2021.
- [8] B. Hu and N. C. Beaulieu, "Pulse shapes for ultra-wideband communication systems," *IEEE Trans. Wireless Commun.*, vol. 4, no. 4, pp. 1789-1797, July 2005.
- [9] A. A. Omar, S. Naser, M. I. Hussein, N. I. Dib, and M. W. Rashad, "Superformula-based compact UWB CPW-fed-patch antenna with and without dual frequency notches," *Appl. Comput. Electromagn. Soc. J.*, vol. 32, no. 11, pp. 979-986, Nov. 2017.

- [10] W. B. Abbas, F. Che, Q. Z. Ahmed, F. A. Khan, and T. Alade, "Device free detection in impulse radio ultrawide bandwidth systems," *Sensors*, vol. 21, no. 9, p. 3255, May 2021.
- [11] D. V. Giri and F. M. Tesche, "Classification of intentional electromagnetic environments (IEME)," *IEEE Trans. Electromagn. Compat.*, vol. 46, no. 3, pp. 322-328, Aug. 2004.
- [12] F. Brauer, S. Fahlbusch, J. L. Haseborg, and S. Potthast, "Investigation of hardening measures for IT equipment against radiated and conducted IEMI," *IEEE Trans. Electromagn. Compat.*, vol. 54, no. 5, pp. 1055-1065, Oct. 2012.
- [13] S. K. Singh, R. Chandra, S. Mitra, R. Kumar, S. Kalyansundaram, A. Roy, J. Mukherjee, and A. Sharma, "High power balanced TEM horn antenna for ultra wide band radiator," *Microwave Opt. Techn. Lett.*, vol. 65, no. 6, pp. 1686-1694, Dec. 2023.
- [14] T. A. Mehlhorn, "National security research in plasma physics and pulsed power: Past, present, and future," *IEEE Trans. Plasma Sci.*, vol. 42, no. 5, pp. 1088-1117, May 2014.
- [15] R. Cicchetti, E. Mioozzi, and O. Testa, "Wideband and UWB antennas for wireless applications: A comprehensive review," *Int. J. Antennas Propag.*, vol. 2017, pp. 1-45, Feb. 2017.
- [16] O. P. Kumar, P. Kumar, T. Ali, P. Kumar, and S. Vincent, "Ultrawideband antennas: Growth and evolution," *Micromachines*, vol. 13, no. 1, p. 60, Dec. 2021.
- [17] D. Potti, Y. Tusharika, M. G. N. Alsath, S. Kirubaveni, M. Kanagasabai, R. Sankararajan, S. Narendhiran, and P. B. Bhargav, "A novel optically transparent UWB antenna for automotive MIMO communications," *IEEE Trans. Antennas Propagat.*, vol. 69, no. 7, pp. 3821-3828, July 2021.
- [18] W. Zhao, T. Jiang, Y. Yan, and B. Wang, "Study on broadening FWHM of combined microwave short-pulse in time domain," in *Int. Conf. Microw. Millim. Wave Technol., ICMMT - Proc.*, Nanjing, pp. 1-3, May 2021.
- [19] T. Latha, G. Ram, G. A. Kuamr, and M. Chakravarthy, "Review on ultra-wideband phased array antennas," *IEEE Access*, vol. 9, pp. 129742-129755, Sep. 2021.
- [20] A. M. Efremov, V. I. Koshelev, B. M. Kovalchuk, V. V. Plisko, and K. N. Sukhushin, "Generation and radiation of ultra-wideband electromagnetic pulses with high stability and effective potential," *Laser Part Beams*, vol. 32, no. 3, pp. 413-418, June 2014.
- [21] V. M. Fedorov, M. V. Efanov, V. Y. Ostashev, V. P. Tarakanov, and A. V. Ul'yanov, "Antenna array with TEM-horn for radiation of high-power ultra short electromagnetic pulses," *Electronics*, vol. 10, no. 9, p. 1011, Apr. 2021.
- [22] S. Foo and S. Kashyap, "Time-domain array factor for UWB antenna array," *Electronics Letters*, vol. 39, no. 18, pp. 1304-1305, Jan. 2003.
- [23] X. Jiang, Y. Yan, L. Meng, B. Wang, L. Bi, and Y. Yin, "Theoretical study on directivity of ultra-wideband time-domain antenna array based on 3D impulse point sources," in *National Conference on Antennas*, Harbin, pp. 816-818, Aug. 2023.
- [24] C. E. Baum, "Radiation of impulse-like transient fields," *Sensor and Simulation Notes*, no. 321, Nov. 1989.
- [25] S. P. Skulkin, V. I. Turchin, N. I. Kascheev, and D. M. Ponomarev, "Transient field calculation of aperture antennas for various field distributions over the aperture," *IEEE Antennas Wirel. Propag. Lett.*, vol. 16, pp. 2295-2298, 2017.
- [26] S. P. Skulkin, N. A. Lysenko, G. K. Uskov, and N. I. Kascheev, "Transient far fields of aperture antennas," *IEEE Antennas Wirel. Propag. Lett.*, vol. 18, no. 5, pp. 1036-1040, May 2019.
- [27] C. A. Balanis, *Antenna Theory: Analysis and Design*. Hoboken: John Wiley & Sons, 2005.
- [28] X. Liu, X. Wang, W. Wang, and Y. Jiang, "Radiant characteristics of subnanosecond and monopolar pulse-excited aperture," *High Power Laser and Particle Beams*, vol. 15, no. 11, pp. 1106-1109, Nov. 2003.
- [29] В. И. Кошелев, В. П. Беличенко, and Ю. И. Буянов, "Ultra-wideband electromagnetic radiation technology," National Defense Industry Press, CN, 2018.
- [30] B. Wang, Q. Liu, H. Cai, T. Jiang, and Y. Yan, "Estimation of time-domain radiation characteristics for dipole antenna array," in *IEEE Int. Conf. Inf. Commun. Networks*, Xi'an, pp. 144-148, Aug. 2023.

Binwen Wang was born in Gansu, China, in 1993. He received his B.S. degree in Nuclear Science from Xi'an Jiaotong University, Xi'an, China, in 2015, and his M.S. degree in Electromagnetic Field and Microwave Technology from the Northwest Institute of Nuclear Technology, Xi'an, China, in 2017. He is currently an Engineer at the Northwest Institute of Nuclear Technology. His research interests include time-domain electromagnetics and ultra-wideband antenna.

Hui Ning was born in Zhejiang, China, in 1969. He received his M.S. and Ph.D. degrees in Nuclear Science and Technology from Tsinghua University, Beijing, China, in 1997 and 2001, respectively. He is currently

a Professor at the Northwest Institute of Nuclear Technology, Xi'an, China, specializing in time-domain electromagnetics and the pulse power technique and its applications.

Chengyun Cao was born in Qinghai, China, in 1994. He received his B.S. and M.S. degree in Electromagnetic Field and Microwave Technology from the National Defense University of Science and Technology, Changsha, China, in 2016 and 2021. He is currently an Engineer at the Northwest Institute of Nuclear Technology, specializing in ultra-wideband antenna.

Qilong Liu was born in Hubei, China, in 1997. He received his B.S. degree in Power System and Automa-

tion from the Army Engineering University of PLA, Shijiazhuang, China, in 2019. He is currently an Assistant Engineer at the Northwest Institute of Nuclear Technology, specializing in ultra-wideband antenna.

Kaiyue Zhang was born in Anhui, China, in 1992. He received his B.S. and M.S. degrees in Electromagnetic Field and Microwave Technology from the National Defense University of Science and Technology, Changsha, China, in 2016 and 2018. He is currently an Engineer at the Northwest Institute of Nuclear Technology, specializing in ultra-wideband antenna and array.